Biosensors and Bioelectronics 138 (2019) 111311

Contents lists available at ScienceDirect

Biosensors and Bioelectronics

journal homepage: www.elsevier.com/locate/bios

A probeless and label-free electrochemical immunosensor for cystatin C detection based on ferrocene functionalized-graphene platform

Erika K.G. Trindade, Bárbara V.M. Silva, Rosa F. Dutra*

Biomedical Engineering Laboratory, Department of Biomedical Engineering. Federal University of Pernambuco, Av. Prof. Moraes Rego, 1235, CEP`50610-970, Recife, Brazil

ARTICLE INFO

Keywords:
Redox probe-free
Cystatin C
Renal failure
Immunosensor
Ferrocene
Graphene

ABSTRACT

A novel electrochemical sensor with inherent redox activity mediated by ferrocene for Cystatin C (CysC), an early kidney failure biomarker, is described. The current response was mediated by graphene oxide-ferrocene nanofilm with redox-activity coming from electroactive species surface-confined. Anti-CysC antibodies were immobilized by their Fc portions on the drop-casting polyethyleneimine (PEI) film for improving the sensitivity and reproducibility. Stepwise modifications of the nanostructured surface were characterized by electrochemical techniques, FT-IR and AFM. FT-IR confirmed the formation of the Fc-GO nanocomposite and PEI deposition on the electrode surface. The AFM micrographs confirmed a nanometric film of Fc-GO and PEI. The sensor platform showed a response from 0.1 to 1000 ng/mL and lower limit of detection (LOD) of 0.03 ng/mL of CysC, with good accuracy, specificity and it was successfully applied for CysC detection. Advantages of this immunosensor include rapid testing with minimal steps by the simple use of an intrinsic redox probe, working in a reduction potential, which avoids potential interferences. This proposal attempts to circumvent amperometric detection limitations and provides a promising candidate for future point-of-care diagnostics without redox probe additional solutions for measurements.

1. Introduction

Studies have shown that the incidence of Acute Kidney Injury (AKI) has been increasing over the last decades and can very likely result in permanent kidney damage (Coca et al., 2012). AKI incidence has been reported to be as high as 20% in the USA and very similar in other countries (Gharaibeh et al., 2018; Hoste et al., 2015). Since AKI is an independent risk factor for Chronic Kidney Disease (CKD), End-Stage Renal Disease (ESRD), cardiac diseases and death, it bears a significant public health concern worldwide (Chawla et al., 2014; Coca et al., 2012; Hoste et al., 2015; Webster et al., 2017). More than half Intensive Care Unit (ICU) patients develop AKI and in-hospital death rates in hospitalized patients with AKI is very high among patients in need of dialysis (Chawla et al., 2014; Hoste et al., 2015). In attempting to increase the chances of patient survival, early detection of renal failure is important and could result in a lower burden for ICU and earlier hospital discharge. Cystatin C (CysC) is a nonglycated 13 kDa protein considered an early marker for AKI related with the glomerular filtration rate (GFR) (Lau et al., 2016; Tao et al., 2016). Evidence has suggested that the increase of serum CysC levels as a marker of renal function may detect kidney dysfunction earlier than creatinine, which is currently the most used diagnostic marker (Gaygisiz et al., 2016). Contrary to creatinine levels, recent studies indicated that serum CysC concentration is more stable and accurate in GFR estimation and is independent of sex, diet and muscle mass (Fox et al., 2014; Mi et al., 2016; Ravn et al., 2017; Shlipak et al., 2013). In this context, the development of a fast and low-cost method for CysC detection is of great importance, aiming to identify early signs of AKI and monitoring of hospitalized patients.

Thus far, a variety of analytic strategies have been used for detection of serum CysC, such as enzyme-linked immunosorbent assay (ELISA), turbidimetric and nephelometric immunoassays (Delanaye et al., 2014; Fonseca et al., 2015; Jiang et al., 2014). However, these are timeconsuming methods and require specialized personnel to operate. Due to this and the great interest in CysC rapid detection, attempts have been made to develop biosensors and immunosensors for CysC. Yang et al. (2016) were able to develop an electrochemical genosensor using gold nanoparticles and iron oxide to amplify the signal. Although the detection limit was low for this work, it is not clinically relevant and the sensor requires many steps for conversion of the signal. Some optical sensors were also developed, such as the work of Gorodkiewicz and Luszczyn (2011) and Tao et al. (2016), which used Surface Plasmon

* Corresponding author.
E-mail address: rosa.dutra@ufpe.br (R.F. Dutra).

https://doi.org/10.1016/j.bios.2019.05.016
Received 1 February 2019; Received in revised form 23 April 2019; Accepted 6 May 2019
Available online 10 May 2019
0956-5663/

Resonance Imaging and Near-Infrared Quantum Dots, respectively, for detection of CysC. The major problem in optical systems is the difficult miniaturization of the methods. In this context, electrochemical amperometric immunosensors have the advantage of specific and sensible detection, easy miniaturization and quick results.

In label-free electrochemical immunosensors, the sensing platform requires transport of the redox species to generate the amperometric signal that is proportional to the diffusion of species on electrode surface hindered by antigen/antibody adsorbed. The redox species are indispensable for label-free electrochemical detection and the most common method is to add the redox species into electrolyte solutions (Wang et al., 2017). One of the drawbacks of this method is that it requires washes and several steps that delay real point-of-care detection. Recently, the focus has been on redox probe-free platform for immunosensing applications (Moreira et al., 2018; Trindade and Dutra, 2018). In this sense, redox active molecules such as ferrocene (Fc) units can be attached to sensor surface as the center for electrochemical activity, dispensing the use of external redox probe as used in conventional immunosensor (Yamanaka et al., 2016). Electrochemistry of ferrocene and its derivatives are well known, and they are appreciated for excellent stability, being of considerable interest in electrochemistry due to the almost reversible oxidation of iron II. This site provides the redox catalytic pair released in electrochemical readings (Fery-Forgues and Delavaux-Nicot, 2000; Lu et al., 2015). The fast electron transfer rate and two-state redox stability are other attractive electrochemical characteristics exhibited by Fc and similar compounds that make them excellent mediators, mainly as used in association with different nanomaterials (Cho et al., 2018; Rabti et al., 2016).

Many strategies based on nanomaterials have been applied in electrochemical immunosensors owing to the improvement of its performances (Amani et al., 2018). Thus far, many nanomaterials have been employed in the development of sensing platforms such as metal oxide nanoparticles (Moreira et al., 2018), noble metal nanoparticles (Vilian et al., 2015) and carbon-based nanomaterials (Roushani and Abdi, 2014). Graphene is a one-atom-thick two-dimensional planar carbon nanosheet. It has attracted attention due to its high surface area and chemical stability. Since the bulk production of graphene is difficult, its derivative Graphene Oxide (GO) is more frequently used due to easy production and presence of functional groups protein-reactive (Rodriguez et al., 2015). Thus, this proof-of-concept study aimed at the functionalization of GO with aminoferrocene (Fc), which appears as an innovative approach to produce a catalytic nanocomposite in order to develop a stable sensor platform. Herein, an electrochemical immunosensor was developed, allowing for Cystatin C detection without the use of redox probes ("redox probe-free").

2. Material and methods

2.1. Reagents

Aminoferrocene (Fc), graphene oxide (GO), polyethyleneimine (PEI), 1-ethyl-3-(3 dimethylaminopropyl) carbodiimide (EDC), N-hydroxysuccinimide (NHS), potassium ferricyanide ($K_3[Fe(CN)_6]$) and potassium ferrocyanide ($K_4[Fe(CN)_6]$) were obtained from Sigma-Aldrich (United States). Cystatin C peptide was obtained from Abcam (United Kingdom). Cystatin C antibody (Anti-CysC) was obtained from Sigma (United States). All other chemicals used were of analytical grade and all the solutions were prepared in ultra-pure water acquired from a Milli-Q station (United States) with a conductivity below 18 MΩ cm^{-1}.

Spiked human serum was used to perform analytical response tests. Serum pool samples were obtained after approval by the Research Ethics Committee of the University of Pernambuco, Brazil. The blood collected from healthy individuals was centrifuged and the serum separated from the blood cells. Positive samples were spiked with CysC diluted in PBS with the same volume to obtain the wished concentrations. Likewise, negative samples were obtained, using the same volume, however without CysC adding. Serum samples were processed and freshly prepared, and all incubations with electrodes were performed at room temperature (approximately 24 °C) at 7.4 pH (Silva et al., 2015).

2.2. Apparatus

Electrochemical measurements were performed in a three-electrode system: helical platinum wire as counter electrode, Ag/AgCl (3 M KCl Sat.) as reference and working gold electrode (GE) (Ø = 1 mm). The electrochemical measurements were performed with a potentiostat/galvanostat Ivium Compact Stat (Eindhoven, Netherlands) coupled to a microcomputer and controlled by the IviumSoft software. Cyclic voltammetry (CV) and square wave voltammetry (SWV) techniques were employed to electrochemically characterize the modifications of the GE. The CV (0.05 V/s scan rate) and SWV (10 Hz frequency and 10 mV pulse amplitude) measurements were carried out at 10 mV step potential with a potential window between −0.3 and 0.2 V in 0.1 M KCl electrolyte.

Morphological analyses of modifications on the GE surface were carried out by means of Atomic Force Microscopy (AFM) in the non-contact mode, using the Nanosurf Flex AFM (Liestal, Switzerland) equipped with a C3000 controller and the TAP190AI-G tip. The images obtained were treated and analyzed by Gwyddion (free version 2.49).

Chemical surface characterization of the platform was accomplished by attenuated total reflectance with Fourier transform infrared spectroscopy (ATR-FTIR) using the Bruker IFS 66 model FT-IR spectrometer (Billerica, USA), set up for spectra from 4000 to 500 cm^{-1}. All AFM images were obtained using a circular gold electrode, with 4 mm diameter made of evaporated gold film onto an acetate sheet.

2.3. Synthesis of PEI/Fc-GO nanostructured surface

Prior to modification, the GE was cleaned by mechanical polishing with 0.5 μm alumina slurry, followed by sonication in distilled water to remove any residual alumina powder. Modifications were performed only after cleaning evaluation with CVs. To confirm GO functionalization, then electrochemical analysis was carried out with three different solutions: GO control, Fc control, and Fc-GO nanocomposite. The Fc-GO nanocomposite was obtained by mixing GO (1 mg/mL, dispersed in water) with Fc in a mixture 1:1 of 20 mM EDC and 50 mM NHS (prepared in acetate buffer 0.037 M, pH 5.0) for 1 h in an ultrasonic bath. Fc concentration was optimized by incubating the GO modified with various concentrations of Fc (0.01; 0.025; 0.05; 0.075; 0.1; 0.2; 0.3 and 0.4 M). The GE surface was modified with 5 μL of the Fc-GO solution by drop casting and dried on the incubator at 50 °C. After the solvent evaporation, the Fc-GO surface was coated with 5 μL of 2% PEI prepared in ethanol and dried at room temperature (approximately 24 °C).

2.4. Immobilization of anti-CysC and analytical measurements

For antibody immobilization, an aliquot (5 μL) of 10 mg/mL anti-CysC solution was pipetted on the nanostructured surface and incubated for 1 h at room temperature (24 °C). In order to block the remaining adsorption-reactive sites, the anti-CysC-immobilized electrode was incubated with a solution of 0.05 M glycine, also prepared in PBS (10 mM, pH 7.4) for 1 h. The electrode was carefully rinsed with distilled water between each step of immunosensor assembly.

The electrochemical detection of CysC was performed by using SWV technique using 0.1 M KCl solution as supporting electrolyte. The as-prepared immunosensor was incubated with 5 μL of CysC peptide PBS diluted at various concentrations (0.1, 1, 10, 50, 100, 500 and 1000 ng/mL) in a moist chamber at 4 °C during 15 min. The analytical response was obtained by the difference of current (ΔI) in the square wave voltammograms (SWV) before (blank) and after the addition of CysC. All graphs and statistical analyses were carried out with Origin Pro 8.0

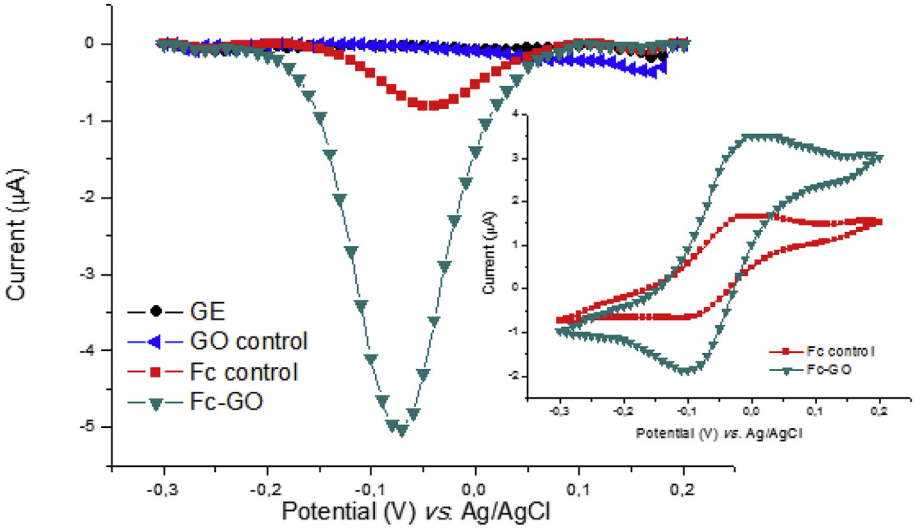

Fig. 1. SWV of the: bare electrode (GE), GO control, Fc control, and Fc-GO nanocomposite; *inset*: CVs of Fc control and Fc-GO nanocomposite showing an increase of electroactive area with Fc-GO nanocomposite.

software.

3. Results and discussion

3.1. Catalytic activity of Fc-GO electrode surface

Fc redox sites generate very distinctive redox pairs with cathodic and anodic peaks at −0.1 V and close to −0.0 V, respectively due to the almost reversible oxidation of iron II, as can be seen in Fig. 1, in which shows SWVs of the bare electrode, GO control, Fc control and Fc-GO nanocomposite, and CVs of Fc control and Fc-GO nanocomposite. All the characterizations were carried out in KCl 0.1 M as supporting electrolyte as means to not interfere with electrochemical activity inherent of Fc. SWV of the bare electrode and GO control show no cathodic peak at the potential attributed to Fc catalytic activity. Furthermore, the functionalization of graphene using Fc allowed for higher electroactive activity than the Fc control, as seen in Fig. 1 and Fig. 1 - *inset*. SWV and CV both showed a current increase after functionalization. This can be attributed to a higher electroactive area provided by GO after stable Fc attachment. The optimal concentration of Fc used for GO functionalization was found at 0.1 M of Fc and used in subsequent experiments based on highest electroactive area.

Fig. 2 (a) shows a schematic representation of nanostructured platform development steps and CV characterization of all the steps is shown in Fig. 2 (b). It can be observed that the deposition of PEI film onto the Fc-GO surface resulted in an increase of 17.8% in the electroactive area compared to Fc-GO (Fig. 2: *inset*). PEI contains a large number of amine groups that act as a crosslinker, attaching the GO by amide bonds while leaving enough amine sites free to bond with the carboxylic groups present at the Fc portion of antibodies. The functionalization of the sensing surface by introducing reactive groups for oriented immobilization of the antibodies is a crucial step to obtain an immunosensor with a high performance (Gomes-Filho et al., 2013). Addition of the antibody, glycine, and readings with CysC resulted in a decrease of the current. This was attributed to electron transfer hindering in the diffusion barrier caused by these molecules, as expected (Valipour and Roushani, 2017).

In presence of 0.1 M KCl, the immobilization of Fc on the graphene was evaluated by scan rate studies varying from 10 to 110 mV/s, at the potential window from −0.3 to 0.2 V **(**Fig. S1 (a)**).** Since the plot of the square root of the scan rate vs. current peak exhibited a linear dependence, with square R of 0.987 and 0.915 for anodic and cathodic peaks, respectively, it was concluded that the process was diffusion-controlled (Fig. S1 (b)). Additionally, by obtaining the plot of scan rate vs. log current as seen in Fig. S1 (c); the slope of cathodic and anodic peaks were 0.48 and 0.57, respectively, confirming that current was controlled by diffusion (Tavares et al., 2013), as also observed by studies with ferrocene moieties adsorbed on polyallylamine film (Jingyuan et al., 2006). This remarkable presence of the faradaic current without redox probe in bulk, with current redox peaks kept at a low potential between −0.1 and 0.0 V, and also the potentials of current peaks that practically did not change seemed to indicate a synergic effect between GO and Fc. Cathodic and anodic peaks (Ipc and Ipa, respectively) increased quasi proportional and symmetrically with scan rate (Fig. S1 (b)), The difference between redox peak potential was less 0.10 V, meaning a voltammetric behavior close to the reversible process (Bard and Faulkner, 2001). Reversibility of the Fc on the nanostructured platform was also evaluated by applying 20 consecutive cycles of CVs in a 0.1 M KCl solution (Fig. S2). The coefficient of variation showed good reproducibility for anodic and cathodic current peaks of 2 and 3%, respectively; arguing the chemical stability of Fc. This good stability was attributed to the covalent bond of the Fc-GO, as confirmed by ATR-FTIR.

AFM was used to characterize the morphology of the electrode. As seen in Fig. 3 (b), (c) and (d), the gold surface was fully covered by layers of the GO control, GO-Fc, and PEI/GO-Fc, respectively, all showing increased average roughness (Ra) when compared with the clean electrode (Ra = 1.00 nm ± 0.02) (Fig. 3 (a)), which exhibited a very smooth and regular morphology. Fig. 3 (c) showed a rougher surface (Ra = 1.80 nm ± 0.03) than that showed in (b) (Ra = 1.63 nm ± 0.03), suggesting that Fc allowed for an increase in surface area, when compared with the GO control (Shearer et al., 2016). The PEI film drop-casted on the GO-Fc nanocomposite surface (Fig. 3 (d)) produced a slight increase in roughness (Ra = 1.89 nm ± 0.04) compared to GO-Fc surface (Lau et al., 2018).

ATR-FTIR has been a valuable technique for biosensors due to allowing the characterization of chemical bonds and functional groups on the surface material. Herein, the spectra obtained at the electrode surface in each step of immunosensor are shown in Fig. 4 as follows: Fc control (spectrum I), Fc-GO nanocomposite (spectrum II) and Fc-GO with PEI (spectrum III). In spectra, I and II, the N–H stretching (ammonium ion) that is usually observed between 3400 and 3300 cm−1 (Fan et al., 2012; Hishikawa et al., 2017; Stuart, 2005) can indicate the presence of the amine groups attributed to Fc. In spectra I, II and III, the bands between 1650 and 1550 cm^{-1} are due to secondary amine (amide II) bending and in spectrum II the asymmetric band at

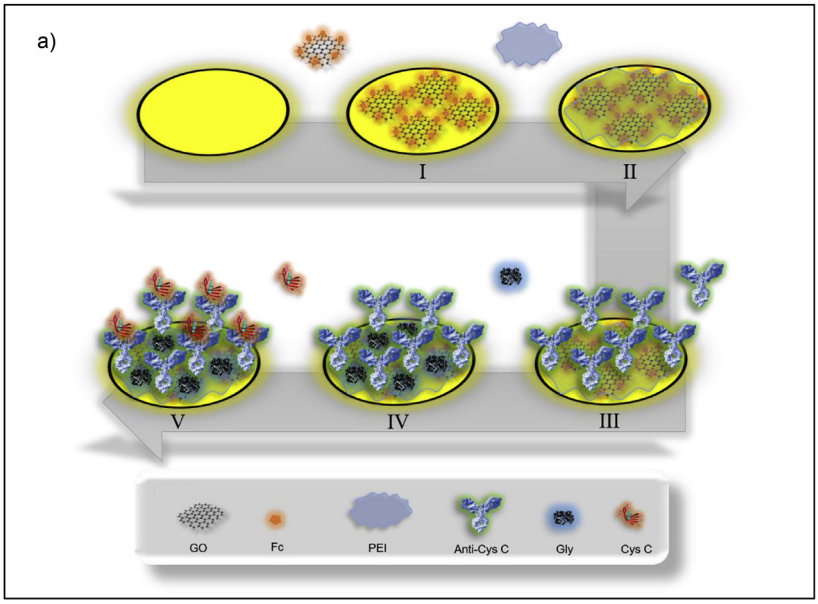

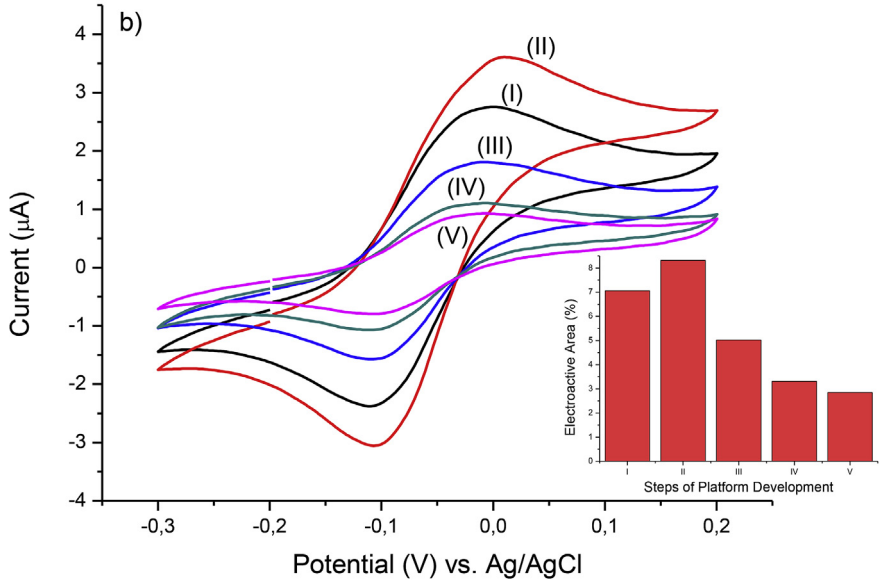

Fig. 2. (a) Schematic representation of nanostructured platform development, **(b)** CVs of each modification step as follows: **(I)** Fc-GO, **(II)** PEI, **(III)** Anti-CysC, **(IV)** Glycine and **(V)** Cys C; *inset:* Plot of steps for platform development *versus* electroactive area of CVs; experiments in presence of 100 mM KCl.

1637 cm^{-1} results from amide I mode (Coates, 2006; Service et al., 2010), that could be attributed to the amide bonds present in the Fc-GO nanocomposite. In spectrum II, the bands between 1242 and 1245 cm^{-1} are due to C–C, C–O and C=O stretch (Fan et al., 2012), then suggesting the presence of GO. In spectrum III, the band found at 1301 cm^{-1} is indicative of amine polymer film on the electrode surface, according to the database from the National Institute of Standards and Technology (U.S. Department of Commerce).

3.2. Analytical responses to the CysC

The analytical performance of the sensor surface was evaluated by submitting the electrode to different concentrations of CysC diluted in PBS (0.1, 1, 10, 50, 100, 500 and 1000 ng/mL). Since the incubation time exerts an important role on the analytical performance, different time incubations were tested, varying from 10 to 45 min, with 15 min adopted as optimal due to steady-state reached, similarly to previous studies (Montes et al., 2016; Singh et al., 2014). The analytical response was obtained by the difference of current (ΔI) in the SWV before and after the addition of CysC samples (Fig. 5 (a)). The analytical curve showed a decrease in the cathodic peaks proportional to CysC concentrations increase (Fig. 5 (b)). This decrease of the current peak is attributed to the hindering in electron transfer by the insulating nature of CysC increasing the diffusion barrier (Dias et al., 2013). The curve of ΔI as function of CysC concentrations exhibited in a monolog plot resulted in a broad range analytical curve linear from 0.1 to 1000 ng/mL (inset Fig. 5 (b)), with linear equation of I (μA) = 0.0045 log [CysC] + 2.63 and LOD of 0.03 ng/mL CysC (3.3 σ). These concentrations in lower values met in clinical reference that is up to 950 ng/mL (Gaygisiz et al., 2016). Therefore, for use samples needs to

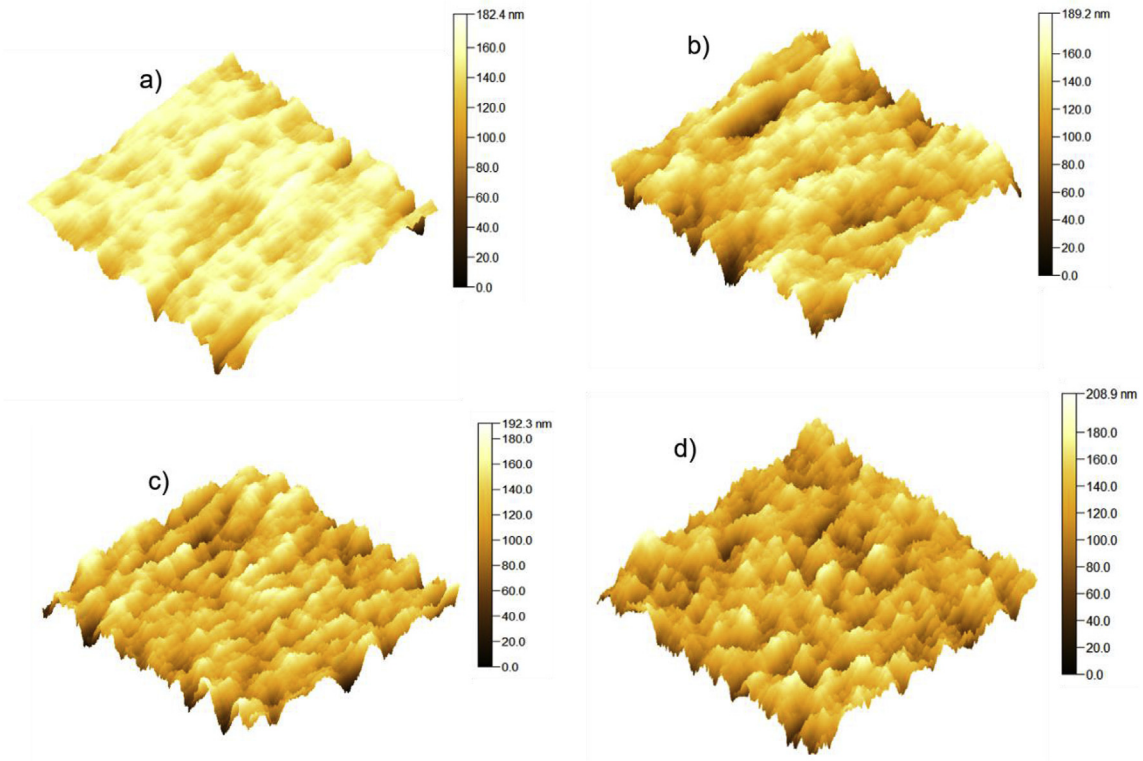

Fig. 3. 3D AFM images of the: **(a)** bare gold electrode (GE), **(b)** GO control, **(c)** Fc-GO nanocomposite and **(d)** addition of PEI.

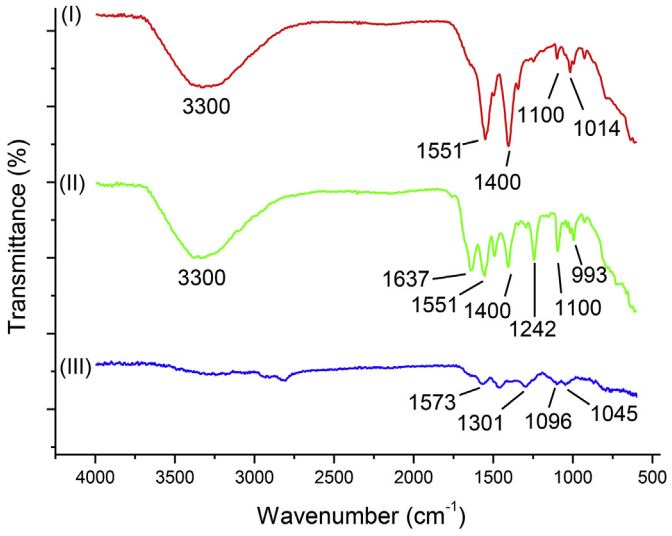

Fig. 4. FT-IR spectra of sensor platform in each step of modifications: Fc control (*spectrum I*), Fc-GO nanocomposite (*spectrum II*) and after PEI drop-casting (*spectrum III*).

be 10 to 100 times diluted in PBS before measurements, with the advantage of minimizing the non-specific bindings.

Different analytical methods for detection of CysC are shown in Table S1 (Sup information). Comparing this immunosensor with all already described for the detection of CysC, it is observed that it presents several advantages. Regarding to the amperometric sensors, this approach is more practical and faster, since it does not require further reading stages, such as the introduction of redox probe solutions and washes (Yang et al., 2016; Desai et al., 2018). While here, the samples can be diluted in PBS or even KCl being ready for reading. Additionally, detection of CysC is directly performed by the antigen-antibody reaction with more advantages, which does not occur with the cited works. In the first, Yang et al. performed the detection via immunoreaction-induced DNA strand displacement and T7 Exonuclease (T7 Exo)-assisted protein cyclic enzymatic amplification. Desai et al.(2018), the second work, developed an assay employing the screen-printed electrode based on K_3 [Fe (CN) $_6$] as an indicator. Although they have achieved an optimal range and a low limit of detection, the use of papain as sensor element, a serine protease that detects enzymatic activity, render the sensor limited for using only in urine. Thus, measurements in samples with protein contaminants like the serum are restrictive, in contrast to this proposed sensor that used antibody Anti-CysC making serological samples feasible, and detections in this fluid are easier and more commonly employed. Optical approaches by using surface plasmon resonance (SPR) was also applied by Gorodkiewicz and Luszczyn (2011) being quite sensitive, however, SPR has the disadvantage of using papain and presents itself as a technology of difficult portability, limiting as point-of-care. Lin et al. (2013) performed an optical detection with nanoparticles using also the papain. Mi et al. (2016) using CysC-specific nanobodies achieved low detection limits in optical transduction based on the photocurrent decrease using an electrochemical workstation to measure photocurrent under visible light irradiation with a 150 W Xe lamp; this application was extended to real sample by monitoring the CysC in human serum samples. Thus, the technology here developed is simpler, and quite liable for a point-of-care diagnostic. To our best knowledge, there are no electrochemical immunosensors for CysC similar to the one here developed.

The matrix effect and selectivity was also tested with this immunosensor by using a real human serum samples, since these complex samples contain a great amount of interferers. Here, it was used a pool of serum, by mixing samples of different volunteers, further increasing the possibility of interferents. As exclusion criteria in samples selections, hemolyzed or hypercholesteremic samples were not included. The assays were carried out by successive incubations with the spiked CysC (10 ng/mL) and non-spiked human serum samples at the same electrode in each experiment (Fig. 6). Analytical responses indicated a gradual decrease in the SWV peaks proportional to the increase of the

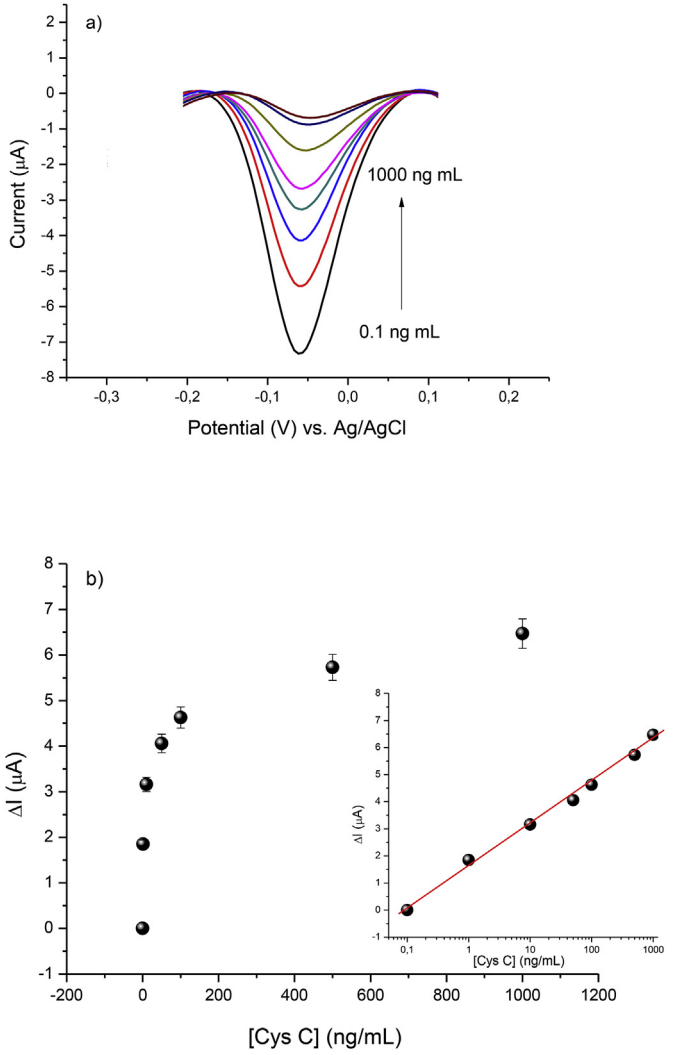

Fig. 5. (a) SWVs responses of immunosensor to the Cys C incubations with analytical detections measured in 100 mM KCl; **(b)** Analytical curve of Cys C antigen in PBS buffer (10 mM, pH 7.4), *inset:* Monolog plot of the Cys C concentration *vs* current variations subtracted from the blank with linear fitting. Bar error represents the standard deviations of three replicate measurements.

CysC concentrations of positive samples, contrary to the non-spiked serum response. Cutoff value was established at mean of negative sample responses plus two deviations, which was found at 20 ng/mL, thus up to this value the immunosensor was able to selectively identify CysC in positive samples, *e.g.* below of this cutoff, the presence of interferences in the samples are significant and can generate positive false.

The nanoimmunonsensor was assessed regarding repeatability (intra-assay) and reproducibility (inter-assay) (Rezaei et al., 2018; Shen et al., 2015). Good repeatability (Figure S3) with a coefficient of variation of 2% was found, using an incubation with concentration of 100 ng/mL CysC and submitting the same electrode to 20 successive SWV readings, with attention to remove the electrode from the electrochemical cell in each reading. Reproducibility tests (Figure S4) were performed showing a good performance, according to the coefficient of variation of relative peak currents of SWV that was found at less than 5% (CV = 4%) obtained by five electrodes prepared in the same conditions applying 100 ng/mL CysC in serum samples. Here, the analytical responses from different electrodes were normalized to compare themselves, *e.g.* SWV fluctuations on the blank from different electrodes due to the charge effect on the electrode by producing different DC current levels were minimized dividing by blank SWV in each electrode.

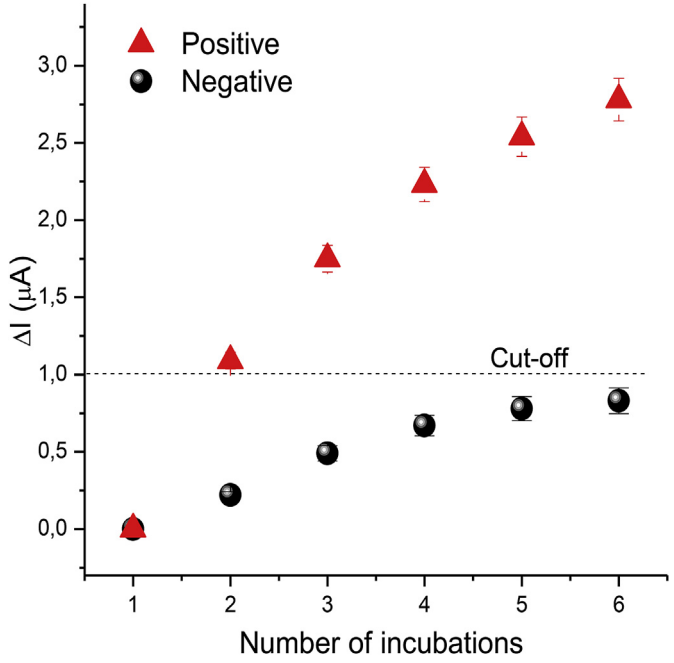

Fig. 6. Matrix effect and selectivity studied in successive incubations in real samples of human spiked serum (with 100 ng/mL Cys C in PBS) and human negative serum (diluted in PBS 10 mM, pH 7.4). Plots represent cathodic peak currents of SWVs subtracted from the blank; SWV measurements performed in presence of 100 mM KCl.

4. Conclusions

A novel electrochemical immunosensor with inherent redox activity mediated by ferrocene was developed. Amperometric responses obtained by SWV were mediated by graphene oxide-ferrocene nanofilm with redox-activity coming from electroactive species surface-confined. As a proof-of-concept, this immunosensor was applied to Cystatin C detection, a biomarker for renal failure. The detection was based on antigen-antibody interaction, differing from most CysC sensors, that have used papain to produce the current responses that allow its application to blood samples and other biological fluids. This platform is simple than optical biosensor to miniaturization and does not need redox probe solutions for measurements, simplifying the steps and being an important advancement towards real point-of-care testings.

Acknowledgments

This research was supported by CNPq Brazilian agencies under grants number 440605/2016-4 , 471065/2014-5 and 407905/2013-8. E. K. G.Trindade thank to the FACEPE and CAPES by her scholarship. The Coordenação de Aperfeiçoamento de Pessoal de Nível Superior – Brazil Code 001, financed this study in part.

Appendix A. Supplementary data

Supplementary data to this article can be found online at https://doi.org/10.1016/j.bios.2019.05.016.

References

Amani, J., Khoshroo, A., Rahimi-nasrabadi, M., 2018. Electrochemical immunosensor for the breast cancer marker CA 15 – 3 based on the catalytic activity of a CuS/reduced graphene oxide nanocomposite towards the electrooxidation of catechol. Microchim. Acta.

Bard, A.J., Faulkner, L.R., 2001. Electrochemical Methods : fundamentals and Applications. Wiley.

Chawla, L.S., Eggers, P.W., Star, R.A., Kimmel, P.L., 2014. Acute kidney injury and

chronic kidney disease as interconnected syndromes. N. Engl. J. Med. 371, 58–66. https://doi.org/10.1056/NEJMra1214243.
Cho, I., Lee, J., Kim, J., Kang, M., Paik, J.K., Ku, S., Cho, H., Irudayaraj, J., Kim, D., 2018. Current technologies of electrochemical Immunosensors : perspective on signal amplification. Sensors (Basel). 18, 1–18. https://doi.org/10.3390/s18010207.
Coates, J., 2006. Interpretation of infrared spectra, a practical approach. Encycl. Anal. Chem. 1–23. https://doi.org/10.1002/9780470027318.a5606.
Coca, S.G., Singanamala, S., Parikh, C.R., 2012. Chronic kidney disease after acute kidney injury: a systematic review and meta-analysis. Kidney Int. 81, 442–448. https://doi.org/10.1038/ki.2011.379.
Delanaye, P., Cavalier, E., Morel, J., Mehdi, M., Maillard, N., Claisse, G., Lambermont, B., Dubois, B.E., Damas, P., Krzesinski, J.-M., Lautrette, A., Mariat, C., 2014. Detection of decreased glomerular filtration rate in intensive care units: serum cystatin C versus serum creatinine. BMC Nephrol. 15, 9. https://doi.org/10.1186/1471-2369-15-9.
Desai, D., Kumar, A., Bose, D., Datta, M., 2018. Ultrasensitive sensor for detection of early stage chronic kidney disease in human. Biosens. Bioelectron. 105, 90–94. https://doi.org/10.1016/j.bios.2018.01.031.
Dias, A.C.M.S., Gomes-Filho, S.L.R., Silva, M.M.S., Dutra, R.F., 2013. A sensor tip based on carbon nanotube-ink printed electrode for the dengue virus NS1 protein. Biosens. Bioelectron. 44. https://doi.org/10.1016/j.bios.2012.12.033.
Fan, M., Dai, D., Huang, B., 2012. Fourier transform infrared spectroscopy for natural fibres. In: Fourier Transform - Materials Analysis, pp. 46–68.
Fery-Forgues, S., Delavaux-Nicot, B., 2000. Ferrocene and ferrocenyl derivatives in luminescent systems. J. Photochem. Photobiol. A Chem. 132, 137–159. https://doi.org/10.1016/S1010-6030(00)00213-6.
Fonseca, I., Reguengo, H., Oliveira, J.C., Martins, L.S., Malheiro, J., Almeida, M., Santos, J., Dias, L., Pedroso, S., Lobato, L., Henriques, A.C., Mendonça, D., 2015. A triple-biomarker approach for the detection of delayed graft function after kidney transplantation using serum creatinine, cystatin C, and malondialdehyde. Clin. Biochem. 48, 1033–1038. https://doi.org/10.1016/j.clinbiochem.2015.07.007.
Fox, J.A., Dudley, A.G., Bates, C., Cannon Jr., G.M., 2014. Cystatin C as a marker of early renal insufficiency in children with congenital neuropathic bladder. J. Urol. 191, 1602–1607. https://doi.org/10.1016/j.juro.2013.09.093.
Gaygisiz, Ü., Aydoıdu, M., Badoılu, M., Boyaci, N., Güllü, Z., Gürsel, G., 2016. Can admission serum cystatin C level be an early marker subclinical acute kidney injury in critical care patients? Scand. J. Clin. Lab. Invest. 76, 143–150. https://doi.org/10.3109/00365513.2015.1126854.
Gharaibeh, K.A., Hamadah, A.M., El-Zoghby, Z.M., Lieske, J.C., Larson, T.S., Leung, N., 2018. Cystatin C predicts renal recovery earlier than creatinine among patients with acute kidney injury. Kidney Int. Reports 3, 337–342. https://doi.org/10.1016/j.ekir.2017.10.012.
Gomes-Filho, S.L.R., Dias, A.C.M.S., Silva, M.M.S., Silva, B.V.M., Dutra, R.F., 2013. A carbon nanotube-based electrochemical immunosensor for cardiac troponin T. Microchem. J. 109. https://doi.org/10.1016/j.microc.2012.05.033.
Gorodkiewicz, E., Luszczyn, J., 2011. Surface plasmon resonance imaging (SPRI) sensor for cystatin determination based on immobilized papain. Protein Pept. Lett. 18, 23–29. https://doi.org/10.2174/092986611794328663.
Hishikawa, Y., Togawa, E., Kondo, T., 2017. Characterization of Individual Hydrogen Bonds in Crystalline Regenerated Cellulose Using Resolved Polarized FTIR Spectra. https://doi.org/10.1021/acsomega.6b00364.
Hoste, E.A.J., Bagshaw, S.M., Bellomo, R., Cely, C.M., Colman, R., Cruz, D.N., Edipidis, K., Forni, L.G., Gomersall, C.D., Govil, D., Honoré, P.M., Joannes-Boyau, O., Joannidis, M., Korhonen, A.-M., Lavrentieva, A., Mehta, R.L., Palevsky, P., Roessler, E., Ronco, C., Uchino, S., Vazquez, J.A., Vidal Andrade, E., Webb, S., Kellum, J.A., 2015. Epidemiology of acute kidney injury in critically ill patients: the multinational AKI-EPI study. Intensive Care Med. 41, 1411–1423. https://doi.org/10.1007/s00134-015-3934-7.
Jiang, R., Xu, C., Zhou, X., Wang, T., Yao, G., 2014. Detection of Cystatin C biomarker for clinical measurement of renal disease by developed ELISA diagnostic kits. J. Transl. Med. 12, 1–8. https://doi.org/10.1186/1479-5876-12-205.
Jingyuan, Chen, Koichi, Aoki, Toyohiko, Nishiumi, Li, T., 2006. Voltammetry of Suspensions of Hollow Particles with Ferrocene-Immobilized Polyallylamine Shells†. https://doi.org/10.1021/LA0610304.
Lau, L., Al-Ismaili, Z., Harel-Sterling, M., Pizzi, M., Caldwell, J.S., Piccioni, M., Lands, L.C., Mottes, T., Devarajan, P., Goldstein, S.L., Bennett, M.R., Zappitelli, M., 2016. Serum cystatin C for acute kidney injury evaluation in children treated with aminoglycosides. Pediatr. Nephrol. 1–9. https://doi.org/10.1007/s00467-016-3450-1.
Lau, S.P., Wong, K.K., Chen, S., Fan, Z., Po, K.H.L., 2018. Polyethylenimine-modified graphene oxide as a novel antibacterial agent and its synergistic effect with daptomycin for methicillin-resistant Staphylococcus aureus. ACS Appl. Nano Mater. 1, 1811–1818. https://doi.org/10.1021/acsanm.8b00219.
Lin, H., Sun, W., Zhao, C., Na, H., 2013. Self-assembly of multiwall carbon nanotubes on sulfonated poly (arylene ether ketone) as a proton exchange membrane. J. Polym. Res. 20, 306. https://doi.org/10.1007/s10965-013-0306-2.
Lu, Y., Jiang, Y., Wu, H., Chen, W., 2015. Ferrocene-functionalized graphene oxide nanosheets: efficient electronic communication between ferrocene centers across graphene nanosheets. Electrochim. Acta 156, 267–273. https://doi.org/10.1016/j.electacta.2015.01.049.
Mi, L., Wang, P., Yan, J., Qian, J., Lu, J., Yu, J., Wang, Y., Liu, H., Zhu, M., Wan, Y., Liu, S., 2016. A novel photoelectrochemical immunosensor by integration of nanobody and TiO2 nanotubes for sensitive detection of serum cystatin C. Anal. Chim. Acta 902, 107–114. https://doi.org/10.1016/j.aca.2015.11.007.
Montes, R., Céspedes, F., Baeza, M., 2016. Highly sensitive electrochemical immunosensor for IgG detection based on optimized rigid biocomposites. Biosens. Bioelectron. 78, 505–512. https://doi.org/10.1016/j.bios.2015.11.081.
Moreira, F.T.C., Rodriguez, B.A.G., Dutra, R.A.F., Sales, M.G.F., 2018. Redox probe-free readings of a B-amyloid-42 plastic antibody sensory material assembled on copper@carbon nanotubes. Sensor. Actuator. B Chem. 264, 1–9. https://doi.org/10.1016/j.snb.2018.02.166.
Rabti, A., Raouafi, N., Merkoçi, A., 2016. Bio(Sensing) devices based on ferrocene-–functionalized graphene and carbon nanotubes. Carbon N. Y. 108, 481–514. https://doi.org/10.1016/j.carbon.2016.07.043.
Ravn, B., Prowle, J.R., Mårtensson, J., Martling, C.-R., Bell, M., 2017. Superiority of serum cystatin C over creatinine in prediction of long-term prognosis at discharge from ICU. Crit. Care Med. 1, 1. https://doi.org/10.1097/CCM.0000000000002537.
Rezaei, B., Shoushtari, A.M., Rabiee, M., Uzun, L., Mak, W.C., Turner, A.P.F., 2018. An electrochemical immunosensor for cardiac Troponin I using electrospun carboxylated multi-walled carbon nanotube-whiskered nanofibres. Talanta 182, 178–186. https://doi.org/10.1016/j.talanta.2018.01.046.
Rodriguez, B.A.G., Trindade, E.K.G., Cabral, D.G.A., Soares, E.C.L., Menezes, C.E.L., Ferreira, D.C.M., Mendes, R.K., Dutra, R.F., 2015. Nanomaterials for advancing the health immunosensor. In: Biosensors - Micro and Nanoscale Applications, pp. 347–374.
Roushani, M., Abdi, Z., 2014. Novel electrochemical sensor based on graphene quantum dots/riboflavin nanocomposite for the detection of persulfate. Sensor. Actuator. B Chem. 201, 503–510. https://doi.org/10.1016/j.snb.2014.05.054.
Service, R.J., Hillier, W., Debus, R.J., 2010. Evidence from FTIR difference spectroscopy for an extensive network of hydrogen bonds near the oxygen-evolving Mn4Ca cluster of photosystem II involving D1-glu65, D2-glu312, and D1-glu329. Biochemistry 49, 6655–6669. https://doi.org/10.1021/bi100730d.Evidence.
Shearer, C.J., Slattery, A.D., Stapleton, A.J., Shapter, J.G., Gibson, C.T., 2016. Accurate thickness measurement of graphene. Nanotechnology 27, 125704. https://doi.org/10.1088/0957-4484/27/12/125704.
Shen, Y., Zhang, Y., Liu, M., Liu, X., Guo, H., Zhang, X., Zhang, C., Li, H., Yao, S., 2015. A simple and sensitive electrochemical immunosensor based on thiol aromatic aldehyde as a substrate for the antibody immobilization. Talanta 141, 288–292. https://doi.org/10.1016/j.talanta.2015.04.004.
Shlipak, M.G., Matsushita, K., Ärnlöv, J., Inker, L.A., Katz, R., Polkinghorne, K.R., Rothenbacher, D., Sarnak, M.J., Astor, B.C., Coresh, J., Levey, A.S., Gansevoort, R.T., 2013. Cystatin C versus creatinine in determining risk based on kidney function. N. Engl. J. Med. 369, 932–943. https://doi.org/10.1056/NEJMoa1214234.
Silva, M.M.S., Dias, A.C.M.S., Silva, B.V.M., Gomes-Filho, S.L.R., Kubota, L.T., Goulart, M.O.F., Dutra, R.F., 2015. Electrochemical detection of dengue virus NS1 protein with a poly(allylamine)/carbon nanotube layered immunoelectrode. J. Chem. Technol. Biotechnol. 90. https://doi.org/10.1002/jctb.4305.
Singh, R., Sharma, A., Hong, S., Jang, J., 2014. Electrical immunosensor based on dielectrophoretically-deposited carbon nanotubes for detection of influenza virus H1N1. Analyst 139, 5415–5421. https://doi.org/10.1039/c4an01335b.
Stuart, B., 2005. Infrared spectroscopy. In: Kirk-Othmer Encyclopedia of Chemical Technology. American Cancer Society. https://doi.org/10.1002/0471238961.0914061810151405.A01.PUB2.
Tao, J., Zhao, P., Zeng, Q., 2016. The determination of cystatin C in serum based on label-free and near-infrared light emitted PbS@BSA QDs. J. Mater. Chem. B 4, 4258–4262. https://doi.org/10.1039/c6tb00080k.
Tavares, E.M., Carvalho, A.M., Gonçalves, L.M., Valente, I.M., Moreira, M.M., Guido, L.F., Rodrigues, J.A., Doneux, T., Barros, A.A., 2013. Chemical sensing of chalcones by voltammetry: trans-Chalcone, cardamonin and xanthohumol. Electrochim. Acta 90, 440–444. https://doi.org/10.1016/J.ELECTACTA.2012.12.040.
Trindade, E.K.G., Dutra, R.F., 2018. A label-free and reagentless immunoelectrode for antibodies against hepatitis B core antigen (anti-HBc) detection. Colloids Surfaces B Biointerfaces 172, 272–279. https://doi.org/10.1016/j.colsurfb.2018.08.050.
Valipour, A., Roushani, M., 2017. Using silver nanoparticle and thiol graphene quantum dots nanocomposite as a substratum to load antibody for detection of hepatitis C virus core antigen: electrochemical oxidation of riboflavin was used as redox probe. Biosens. Bioelectron. 89, 946–951. https://doi.org/10.1016/j.bios.2016.09.086.
Vilian, a. T.E., Veeramani, V., Chen, S.-M., Madhu, R., Kwak, C.H., Huh, Y.S., Han, Y.-K., 2015. Immobilization of myoglobin on Au nanoparticle-decorated carbon nanotube/polytyramine composite as a mediator-free H2O2 and nitrite biosensor. Sci. Rep. 5, 18390. https://doi.org/10.1038/srep18390.
Wang, H., Gao, X., Ma, Z., 2017. Multifunctional substrate of label-free electrochemical immunosensor for ultrasensitive detection of cytokeratins antigen 21-1. Sci. Rep. 7, 1–7. https://doi.org/10.1038/s41598-017-01250-0.
Webster, A.C., Nagler, E.V., Morton, R.L., Masson, P., 2017. Chronic kidney disease. Lancet 389, 1238–1252. https://doi.org/10.1016/S0140-6736(16)32064-5.
Yamanaka, K., Vestergaard, M.C., Tamiya, E., 2016. Printable electrochemical biosensors: a focus on screen-printed electrodes and their application. Sensors (Switzerland) 16, 1–16. https://doi.org/10.3390/s16101761.
Yang, Z.H., Zhuo, Y., Yuan, R., Chai, Y.Q., 2016. Highly effective protein converting strategy for ultrasensitive electrochemical assay of cystatin C. Anal. Chem. 88, 5189–5196. https://doi.org/10.1021/acs.analchem.6b00210.